ChemPubSoc Europe

DOI: 10.1002/cphc.201900072

CHEMPHYSCHEM Articles

Hexacoordinated Tetrel-Bonded Complexes between TF_4 (T=Si, Ge, Sn, Pb) and NCH: Competition between σ- and π-Holes

Mariusz Michalczyk,*[a] Wiktor Zierkiewicz,*[a] Rafał Wysokiński,[a] and Steve Scheiner*[b]

In order to accommodate the approach of two NCH bases, a tetrahedral TF_4 molecule (T=Si, Ge, Sn, Pb) distorts into an octahedral structure in which the two bases can be situated either *cis* or *trans* to one another. The square planar geometry of TF_4, associated with the *trans* arrangement of the bases, is higher in energy than its see-saw structure that corresponds to the *cis* trimer. On the other hand, the square geometry offers an unobstructed path of the bases to the π-holes above and below the tetrel atom and hence enjoys a higher interaction energy than is the case for the σ-holes approached by the bases in the *cis* arrangement. When these two effects are combined, the total binding energies are more exothermic for the *cis* than for the *trans* complexes. This preference amounts to some 3 kcal mol^{-1} for Sn and Pb, but is amplified for the smaller tetrel atoms.

1. Introduction

The replacement of the bridging proton of a H-bond with one of several electronegative atoms leads to the concept of parallel noncovalent interactions, with names like halogen, chalcogen, or pnicogen bonds, depending upon the family of the periodic table from which the substitute bridging atom is drawn.[1–4] These noncovalent bonds, sometimes generically referred to as σ-hole interactions due to the deficiency of electron density that lies directly opposite a covalent bond in which the bridging atom is involved[5–7] have been extensively studied over the last few years and are consequently rather well understood. Closely related to these interactions are those in which the bridging atom comes from the tetrel family (C, Si, Ge, etc). These tetrel bonds differ a bit from the others in this set of noncovalent bonds primarily in that the central atom is typically covalently bonded to four substituents, as compared to only one for a halogen bond or as many as three for a pnicogen bond. This larger number of substituents obstructs a clear passage of an approaching nucleophile toward the tetrel atom,[8] which can inhibit the formation of such a bond or at the least require a good deal of deformation so as to clear a space for the Lewis base. Despite any barriers to their formation, these tetrel bonds occur widely and are of great import in a number of chemical and biological processes. This sort of bond can, for example, be considered a preliminary step in the very common S_N2 reaction.[9,10] Scores of tetrel bonds have been identified within protein structures,[11–15] and are implicated in the catalytic process of several enzymes.[16–21]

There is a rapidly growing literature[22–27] that has provided a wealth of insights into the chemical and physical phenomena that underlie tetrel bonds. It is known for example, that the tetrel bond formed by a TR_4 molecule (T = tetrel atom) is strengthened by increasing electron-withdrawing capacity of the R substituent,[28–30] as well as increasing size of the T atom (i.e. C < Si < Ge).[31–34] This strengthening is amplified when either molecule acquires an electric charge.[35–42] The scale and effects of the geometric deformation of the TR_4 molecule required to accommodate a Lewis base have been assessed quantitatively.[43–46] There has also been some consideration of the rather unusual bases carbenes[47,48] or π-systems[33] as tetrel bond acceptors. Finally, there has been some inquiry[49,50] as to how spectral data might be interpreted so as to identify the presence of tetrel bonds and to quantify their strength.

It would appear then that there is currently available a good deal of information concerning the forces and issues relating to the formation of a tetrel bond. But the question arises as to whether a tetrel atom, within a tetravalent covalent bonding situation, is limited to only a single such bond. Is it possible for a tetrel (T) atom in a TR_4 molecule to engage in a pair of tetrel bonds simultaneously, and if so how would the properties of two such bonds differ from a single bond? The theoretical literature to date has little to say on this issue. Some recent work considered unusually structured Pb Lewis acids including hypervalent Sn[51] or Pb atoms in situations where the coordinating groups lie on only one side of the Pb atom .[52–54] Other work looked at the situation from the opposite perspective, viz. two tetravalent tetrel atoms engaging in numerous tetrel bonds with a single base.[25,55–60] There has been a certain amount of consideration of the general topic of

[a] M. Michalczyk, Dr. W. Zierkiewicz, Dr. R. Wysokiński
Faculty of Chemistry
Wrocław University of Science and Technology
Wybrzeże, Wyspiańskiego 27, 50-370 Wrocław, Poland
E-mail: mariusz.michalczyk@pwr.edu.pl
wiktor.zierkiewicz@pwr.edu.pl
[b] Prof. S. Scheiner
Department of Chemistry and Biochemistry
Utah State University
Logan, Utah 84322-0300, United States
E-mail: steve.scheiner@usu.edu

Supporting information for this article is available on the WWW under https://doi.org/10.1002/cphc.201900072

hypervalent pnicogen, halogen, and even aerogen atoms[9,61–74] but not in the context of tetrel atoms, which have their own unique electronic and spatial issues.

Steric crowding notwithstanding, there is clear precedent for the formation of two simultaneous tetrel bonds within the context of elucidated crystal structures. Upon binding of two ligands to a tetracoordinated molecule, one might expect the resulting complex to take on at least some of the geometric characteristics of a hexacoordinated octahedron. That being the case, the two incoming ligands could take up positions either *cis* or *trans* to one another. And indeed, a survey of the CSD (Cambridge Structural Database)[75] provides a number of examples of crystal structures with hexacoordinated tetrel (T) atoms that include a pair of Lewis base ligands. Figure S1 displays a wide array of sample structures, two of which are illustrated as examples in Figure 1, both with T=Ge.

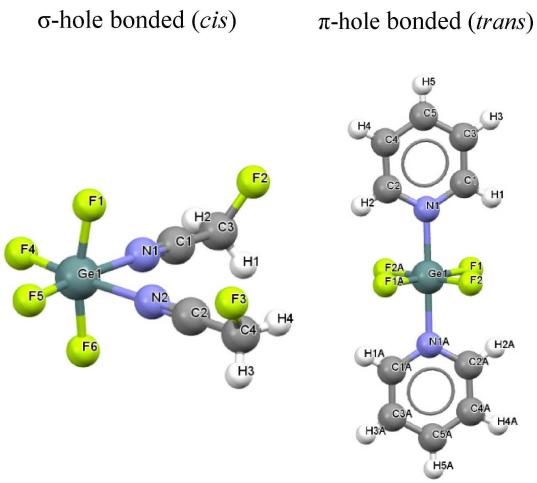

Figure 1. Representative crystal structures of tetrel bonded complexes with hexacoordinated central tetrel Ge atom in two binding modes: *cis* (left) and *trans* (right).[76,77]

The two NC≡CFH$_2$ units are *cis* to one another in AYURET[76] in what might be deemed equatorial locations. As such they each occupy a position directly opposite an equatorial F atom, a so-called σ-hole along the F–Ge axis. In contrast, the two pyridine ligands are directly opposite one another, in *trans* or axial positions in HUMCOH.[77] Each base thus lies above or below the GeF$_4$ plane, attracted by a π-hole of that unit.

These observations lead to a natural set of questions. In the first place, are both of these sorts of structures stable in their own right, or is one or the other a product of the crystalline environment in which the system finds itself? If both are indeed possible structures, what factors favor one over the other, and how much do they differ in energy? How strongly does each geometry bind the two bases, i.e. what sorts of tetrel bond energies are associated with this pair of noncovalent interactions? How much energy must be invested into the deformation of the T-containing molecule to rearrange itself so as to accommodate the two approaching nucleophiles? Is there an energetically feasible route for the rearrangement from *cis* to *trans* geometry? The results presented here represent an attempt to answer these questions via high-level quantum calculations.

1.1. Computational Details

A full set of TF$_4$ molecules were chosen as the tetrel atom-containing monomer, with T=Si, Ge, Sn and Pb. The electron-withdrawing F substituents facilitate the formation of tetrel bonds, and the symmetry associated with four identical substituents allow focus to be drawn to the central question of comparison of two possible overall structures of the complexes. NCH was taken as the universal Lewis base. Its N atom provides a reasonably strong Lewis base, while the linearity of this molecule mitigates against any secondary interactions that might otherwise occur with the F substituents, or between the two bases themselves, that would complicate the analysis.

Full geometry optimizations were carried out for isolated monomers as well as complexes at two levels of theory: MP2/cc-pVTZ[78,79] and BLYP–D3/Def2TZVPP. Single point computations, using the MP2 optimized geometries, were also performed with the CCSD(T)/cc-pVTZ protocol.[80–84] The cc-pVTZ-PP pseudopotential (from ESML libraries) was applied to Sn and Pb so as to capture relativistic effects.[85,86] For the complexes investigated vibrational analyses confirmed the identity of true minima (no imaginary frequencies). The binding energy of each complex was calculated as the energy difference between the complex and the sum of the individually optimized monomers. The interaction energy takes as its reference the energies of the monomers computed in the geometries obtained within the complex. The deformation energy, defined as the energy required to distort each monomer from its optimized geometry to that within the dimer, was defined as the difference between electronic energies of monomer in two geometries: within the complex and fully isolated. Both interaction and binding energies were corrected for basis set superposition error (BSSE) using the Boys-Bernardi procedure.[87]

Computations was carried out with the Gaussian 09 software.[88] Energy decomposition analysis (EDA) was performed at the BLYP-D3/ZORA/TZ2P level implemented in ADF software using the DFT geometries.[89–91] The molecular electrostatic potentials (MEPs) of the isolated monomers were designated on the electron density isosurfaces of $\rho = 0.001$ a.u. at the MP2/cc-pVTZ level and their extrema were evaluated using the WFA-SAS and MultiWFN programs.[92–94] MP2 electron densities were analyzed by the AIMAll program to identify bonding paths between interacting subunits.[95] NBO analysis was employed to analyze interorbital interactions and charge transfer using the BLYP geometries.[96]

2. Results

2.1. Properties of TF_4 Monomers

Values of the maxima of molecular electrostatic potentials ($V_{s,max}$) of the isolated and fully optimized tetrahedral TF_4 (T=Si, Ge, Sn or Pb) are collected in the second column of Table 1.

Table 1. Maxima of molecular electrostatic potentials ($V_{x,max}$) on the 0.001 a.u. contour of the electron density of isolated TF_4 (T=Si, Ge, Sn, Pb) in tetrahedral, see-saw, and planar geometries, and the difference in energy between the two latter geometries and tetrahedral. Calculated at the MP2/cc-pVTZ level of theory. All quantities in kcal/mol.

	$V_{s,max}$ σ-hole tetrahedral	E(see-saw)-E (tet)	$V_{s,max}$ σ-hole see-saw	E(planar)-E (tet)	$V_{s,max}$ π-hole planar
SiF_4	41.3	96.64	127.3	63.53	109.8
GeF_4	50.9	75.51	120.9	49.65	106.1
SnF_4	70.1	52.70	129.4	31.92	121.3
PbF_4	63.6	36.67	127.3	21.97	104.1

Each maximum occurs directly opposite a F atom, so is designated as a σ-hole. The values increase as the tetrel atom size increases, passing through a maximum for T=Sn.[44]

The CSD survey had indicated that when TF_4 is coordinated to a pair of Lewis bases, the entire structure adopts an octahedral shape (see Figure S1). The two bases can be positioned either *cis* or *trans* to one another. In the former case, the TF_4 segment adopts what might be termed a see-saw shape, with two of the F atoms in axial positions, and the other two F are equatorial, as indicated in Figure 2.

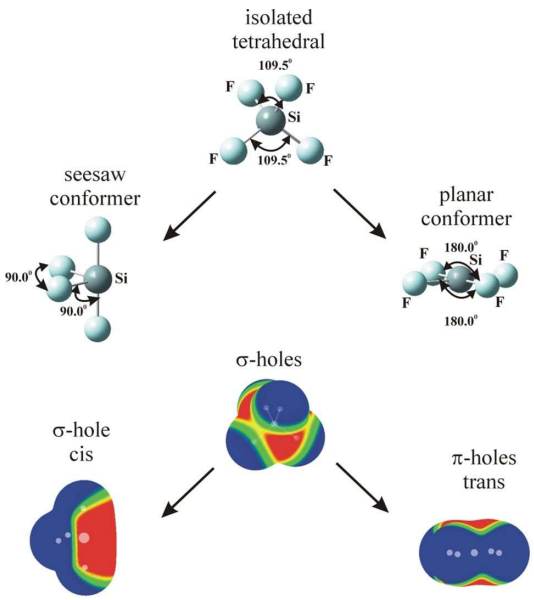

Figure 2. MEP isosurfaces (on the ρ = 0.001 a.u. isodensity surface at the MP2/cc-pVTZ level) of the three idealized geometries of TF_4 monomers (T=Si, Ge, Sn, Pb): isolated optimized tetrahedral, seesaw conformer (initial structure for σ-hole attack) and planar conformer (initial structure for π-hole attack).

Optimizing the geometries of such a see-saw shape of each TF_4 molecule, with θ(FTF) angles of 90°, 120°, and 180°, of course results in a much higher energy than the tetrahedral structure. This difference in energy, displayed in Table 1, is nearly 100 kcal/mol for SiF_4, and then drops steadily as T grows in size. The positions directly opposite the two equatorial F atoms are of σ-hole type, illustrated by the red area of Figure 2. The transition from tetrahedral to see-saw greatly amplifies $V_{s,max}$ to over 120 kcal/mol, with little differentiation with respect to T.

The positioning of the two ligands opposite one another leaves TF_4 in a planar structure as in Figure 2. Optimization of the D_{4h} geometry leads to energies higher than the tetrahedral structure, but not as much as the see-saw geometry. The energy required to distort from tetrahedral to planar drops from 64 kcal/mol for SiF_4 down to 22 kcal/mol for T=Pb. The planar structure contains a pair of MEP maxima, each directly above and below the molecular plane, indicated by the red regions in Figure 2. As may be seen in Table 1, $V_{s,max}$ is quite a bit larger for these π-holes than for the σ-holes of the tetrahedral geometries. The pattern of these maxima for the π-holes differs from the tetrahedral σ-hole pattern: the intensity drops slowly as T grows larger, with the exception of a significant bump for T=Sn. Figure S2 quantifies the increase in $V_{s,max}$ during the transition from tetrahedral to planar, from σ to π-hole.

In summary, the distortion from tetrahedral to the see-saw is considerably more costly than to planar, which would thus favor the *trans* positioning of the two Lewis base ligands over the *cis* arrangement. On the other hand, the σ-holes within the see-saw structure are more intense than the π-holes associated with the planar geometry, which ought to preferentially strengthen the interactions of the *cis* arrangement.

2.2. Complexes

2.2.1. Geometries and Energies

Consistent with observations in numerous crystals, two different geometries are obtained when a pair of NCH Lewis bases are allowed to interact with TF_4. The *cis* placement of the bases results in a distorted octahedron, as illustrated in Figure 3a, wherein there are two types of F atoms.

The F_a designation refers to the axial F atoms, whereas the F_e atoms are equatorial within this skeleton. Each NCH molecule lies approximately opposite one of the T–F_e covalent bonds, along a σ-hole, in an equatorial position. All F atoms are equivalent to one another when the two NCH ligands lie opposite each other in axial positions, in Figure 3b. These ligands occupy π-holes in the square planar TF_4 unit.

The binding energies of the pair of NCH molecules to each TF_4 molecule are displayed in Table 2. This quantity is fairly small for the two smaller tetrel atoms. Indeed, it is even positive for the *trans* Si and Ge structures, indicating the complex is higher in energy than the three separate optimized monomers. However, the binding is considerably stronger for the two heavier T atoms, with little distinction observed between Sn

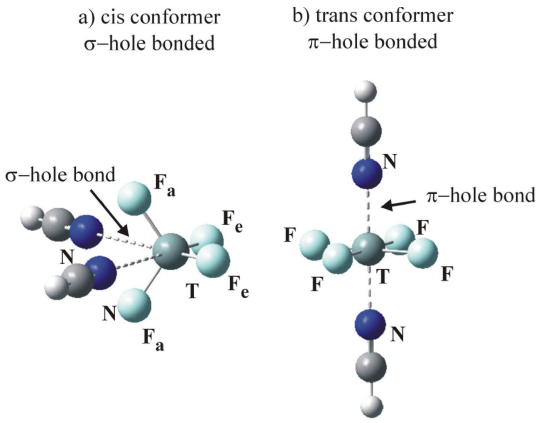

Figure 3. Optimized structures of a) *cis* and b) *trans* conformers of TF_4 complexes with HCN.

Table 2. Binding energies (E_b, kcal mol^{-1}) of TF_4 complexes with 2 NCH calculated at the MP2/cc-pVTZ (I), BLYP–D3/Def2TZVPP (II) and CCSD(T)/cc-pVTZ (III) levels of theory.

	cis			*trans*		
	(I)	(II)	(III)	(I)	(II)	(III)
$(HCN)_2\cdots SiF_4$	−3.33	−3.47	−3.18	19.68	22.33	20.64
$(HCN)_2\cdots GeF_4$	−5.07	−5.13	−4.82	6.95	5.67	7.85
$(HCN)_2\cdots SnF_4$	−17.76	−14.78	−16.80	−14.49	−11.85	−13.86
$(HCN)_2\cdots PbF_4$	−17.16	−15.06	−15.75	−14.43	−13.46	−13.24

and Pb. With respect to level of theory, MP2 (I) and CCSD(T) (III) treatments of electron correlation provide quite similar values, indicating stronger binding than does the BLYP-D3 DFT functional (II).

The *cis* equatorial structure is more stable than the *trans* axial geometry in all cases. The energetic advantage of the former over the latter is listed in Table 3 at two different levels of theory. Whether MP2/cc-pVTZ or BLYP-D3/Def2TZVPP, the energy difference is greatest for T=Si and diminishes as the tetrel atom grows larger, changing from about 23 kcal/mol for SIF_4 and dropping to 2 kcal/mol for Pb. These trends in electronic energy are consistent with the Gibbs free energies, in parentheses in Table 3.

The relative stabilities in Table 3 parallel the energetics of the monomers in Table 1. Specifically, the planar geometry of SiF_4 is higher in energy than the see-saw structure by 33 kcal/mol, a difference which progressively diminishes as T becomes larger, dropping to 15 kcal/mol for T=Pb. This same pattern, albeit with smaller quantitative values, applies to the *trans* vs *cis* complexes in Table 2, so it is apparent that the different energies of deformation of the TF_4 monomer bear a direct causal relation to the relative stabilities of the two types of complexes.

Table 3. Electronic energies and Gibbs free energies (kcal mol^{-1}), corrected for BSSE[a], of *trans* complex relative to the *cis* structure of TF_4 complexes with 2 HCN calculated at the MP2/cc-pVTZ (I), BLYP-D3/Def2TZVPP (II) levels of theory.

	(I)	(II)
$(HCN)_2\cdots SiF_4$	23.01 (30.95)[b]	25.80 (34.12)
$(HCN)_2\cdots GeF_4$	12.02 (17.46)	10.80 (17.04)
$(HCN)_2\cdots SnF_4$	3.27 (3.30)	2.93 (3.86)
$(HCN)_2\cdots PbF_4$	2.73 (2.29)	1.60 (2.04)

[a] All values were corrected for corresponding differences between trans and cis BSSE corrections. [b] Gibbs free energies in parentheses.

The interaction energy is defined as the energy of the complex relative to that of the three monomers, once the latter have already been deformed to the geometries they adopt within the fully optimized trimer. E_{int} is thus more exothermic than is E_b, as reported in Table 4.

Table 4. Interaction energies (E_{int}, kcal mol^{-1}) corrected for BSSE of TF_4 complexes with 2 NCH calculated at the MP2/cc-pVTZ (I), BLYP-D3/Def2TZVPP (II), and CCSD(T)/cc-pVTZ (III) levels of theory.

	cis			*trans*		
	(I)	(II)	(III)	(I)	(II)	(III)
$(HCN)_2\cdots SiF_4$	−3.77	−3.87	−3.63	−46.49	−40.43	−45.46
$(HCN)_2\cdots GeF_4$	−7.10	−6.25	−6.81	−44.65	−36.10	−43.43
$(HCN)_2\cdots SnF_4$	−33.29	−25.06	−32.06	−47.51	−37.58	−46.48
$(HCN)_2\cdots PbF_4$	−26.28	−20.76	−24.59	−36.30	−29.55	−34.71

First with respect to the *cis* complexes, some of the trends of E_b remain intact in E_{int}, for example the stronger binding of the T=Sn and Pb trimers. But one difference emerges in that the interaction energies for Sn are considerably larger than for Pb, despite the larger size of the latter. Where E_b and E_{int}, differ most is in the axial complexes, where the latter quantity is far more negative than is the former. Also, whereas E_b was clearly less attractive for the smaller T atoms, even positive in sign, the interaction energies show surprisingly little dependence upon T. Indeed, it is PbF_4 which shows the least negative E_{int}, opposite to E_b which was least attractive for Si.

These striking differences between E_b and E_{int} are traced to the deformation energies which are presented in Table 5. Deformation energies within the pair of NCH monomers are negligible, 0.3 kcal/mol or less, so these values are almost exclusively due to the TF_4 molecules. These quantities are fairly small, 2 kcal/mol or less for the *cis* Si and Ge complexes, but grows larger for Pb and is maximized for the Sn structures, up to as much as 15 kcal/mol. In other words, the stronger intrinsic binding of Sn over Pb is washed out by the larger deformation energy of the former, resulting in nearly equal values of E_b. The story is very different for the *trans* complexes which require enormous deformation energies. Note also that these quantities are largest for the small Si tetrel atom, and are progressively

Table 5. Deformation energies (E_{def}, kcal mol^{-1}) of monomers preparatory to forming complexes, calculated at the MP2/cc-pVTZ (I), BLYP-D3/Def2TZVPP (II), and CCSD(T)/cc-pVTZ (III) levels of theory.

	cis			*trans*		
	(I)	(II)	(III)	(I)	(II)	(III)
$(HCN)_2\cdots SiF_4$	0.44	0.40	0.45	65.67	62.76	66.10
$(HCN)_2\cdots GeF_4$	2.03	1.12	1.99	51.60	41.77	51.28
$(HCN)_2\cdots SnF_4$	15.53	10.28	15.26	33.02	25.73	32.62
$(HCN)_2\cdots PbF_4$	9.12	5.70	8.84	21.87	16.09	21.47

Table 6. Structural parameters (Å and degrees) in TF_4 complexes with 2 HCN at the MP2/cc-pVTZ level.

	R(N···T) *trans*	R(N···T) *cis*	θ(F_a–T–F_a) *cis*	θ(F_a–T–F_e) *cis*	θ(F_e–T–F_e) *cis*	θ(F_e–T···N) *cis*	θ(N–T···N) *cis*
$(HCN)_2$···SiF_4	2.011	3.201	112.7	109.3	106.5	177.9	110.7
$(HCN)_2$···GeF_4	2.096	2.897	118.6	108.4	103.7	177.6	108.6
$(HCN)_2$···SnF_4	2.278	2.373	148.8	99.5	104.3	170.8	86.0
$(HCN)_2$···PbF_4	2.421	2.494	147.2	99.8	106.0	169.7	85.4
pure octahedron			180	90	90	180	90

reduced as T grows larger. Since E_{int} depicts a rough independence of native interaction upon the identity of T, it is therefore the lower deformation energies of the larger T atoms which yield their more negative binding energies. And it is these very large deformation energies of the *trans* complexes which make them less stable than their *cis* congeners, a trend which is amplified for the smaller Si and Ge atoms.

Examination of some of the geometrical aspects of the two sorts of complexes add some insight into their binding characteristics and energetics. The first two columns of Table 6 indicate that the NCH gets much closer to the central T atom in the *trans* structures.

In $(HCN)_2$···SiF_4, for example, the R(N··Si) distance in the *trans* structure is only 2.01 Å, as compared to 3.20 Å in the *cis* geometry. This closer approach in the *trans* structures echoes the much more negative values of E_{int}. As the T atom grows larger, the R(N···T) distance elongates for the *trans* structure, consistent with the larger T atomic radius. But this same distance changes in the opposite way, becoming shorter for the *cis* complexes, with a minimum for Sn, again consistent with the most negative E_{int} for the *cis* complexes. These quantities are all much shorter than the Alvarez-deduced sum of van der Waals radii[97] of the corresponding atoms (the N···Si, N···Ge and N···Sn distances are: 3.85, 3.95 and 4.08 Å, respectively).

The succeeding columns of Table 6 report various internal angles within each *cis* complex. The last row displays the values that one would expect if this structure adopted a purely octahedral structure, characteristic of the *trans* complexes, with which the actual values may be compared. The deviation from octahedral structure is perhaps most obvious with respect to the θ(F_a–T–F_a) angle in that the two axial F_a atoms bend down toward one another, as this angle is much smaller than the octahedral value of 180°. This bending is most severe for Si and Ge with a F_a–T–F_a nonlinearity of 61–67°. This same bending permits the two F_a atoms to move further away from F_e, with θ(F_a–T–F_e) angles larger than 90°. The two F_e atoms move away from each other as well, with θ(F_e–T–F_e) also exceeding 90° by some 14–17°. The nature of these *cis* structures as σ-bonded complexes is evident in that the θ(F_e–T···N) angles are not very different from 180°. The θ(N–T···N) angles underscore a difference between the smaller and larger tetrel atoms. The two NCH molecules avoid one another with θ(N–T···N) larger than 90° for T=Si or Ge, but come closer for Sn and Pb.

Many of the trends in the deformation energies can be traced to deviations of the θ(F–T–F) angles from the tetrahedral 109.5° in the optimized monomer. In the first place, the 90° and 180° angles in the *trans* structures deviate quite a bit more from the idealized tetrahedral angle than do the values reported for the *cis* complexes in Table 6, consistent with the much larger deformation energies of the former. And the squeezing together of the tetrahedral arrangement to 90° separations in the *trans* geometries would have stronger repercussions for the smaller T atoms for which the F atoms are clustered closer together by shorter T–F covalent bonds. With respect to the *cis* structures, the θ(F–T–F) angles are closest to 109.5° for Si, followed closely by Ge, then a big gap for the bigger Sn and Pb with much larger deviations, mirroring the trends in E_{def}. Within this subgroup of bigger Sn and Pb atoms, these deviations have a larger effect for the smaller Sn atom with its shorter T–F bonds.

2.2.2. Analysis

The partitioning of the total interaction energy of each complex into its constituent parts reveals fundamental similarities and differences amongst them. Although the numerical values differ from one complex to the next, the electrostatic contribution accounts for roughly 60% of the total attractive energy in the *cis* complexes, and a slightly smaller amount to the *trans* structures, as detailed in Table 7.

In fact, this percentage rises steadily as the T atoms grows larger for the *trans* complexes. Orbital interactions are fairly variable for the *cis* structures, rising from 14% for SiF_4 up to 37% for SnF_4. The pattern reverses itself for the *trans* complexes where E_{oi} drops as T becomes larger, but the orbital interactions make up approximately 40% of the total attraction, generally a larger proportion than in the *cis* trimers. Dispersion is quite small, less than 5%. The only exceptions are the *cis* complexes involving Si and Ge, where E_{disp} soars to as much as 26%, compensating for their small orbital interactions.

The properties of the AIM bond critical points are typically a reliable measure of the strength of a given noncovalent bond, although there are exceptions. The molecular diagrams of the relevant trimers are presented in Figure S3, and three key properties of each bond critical point are contained in Table 8.

Some of the trends in Table 8 indeed conform to the interaction energies. For example, the AIM treatment of the *trans* structures adequately reflects E_{int}, both of which suggest a near equivalence of T···N bond strengths, with Pb···N the weakest. The somewhat stronger Sn···N and Pb···N bonds of the *trans* structures, as compared to *cis*, is borne out by AIM data. There are also exceptions to this parallel behavior as well. Taking the *cis* complexes as an example, both ρ and $\nabla^2\rho$ are at

Table 7. EDA/BLYP-D3/ZORA/TZ2P decomposition of the interaction energy of *cis* and *trans* complexes into Pauli repulsion (E_{Pauli}), electrostatic (E_{elec}), orbital interaction (E_{oi}) and dispersion (E_{disp}) terms. All energies in kcal/mol. The relative values in percent express the contribution of each to the sum of all attractive energy terms.

Complex	E_{int}	E_{Pauli}	E_{elec}	%	E_{oi}	%	E_{disp}	%
cis								
$(HCN)_2\cdots SiF_4$	−4.87	6.73	−6.94	60	−1.58	14	−3.07	26
$(HCN)_2\cdots GeF_4$	−7.63	12.31	−12.34	62	−4.10	21	−3.50	18
$(HCN)_2\cdots SnF_4$	−27.45	64.91	−54.30	59	−34.37	37	−3.69	4
$(HCN)_2\cdots PbF_4$	−22.85	46.98	−41.68	60	−24.51	35	−3.64	5
trans								
$(HCN)_2\cdots SiF_4$	−42.80	141.82	−95.67	52	−84.45	46	−4.49	2
$(HCN)_2\cdots GeF_4$	−37.60	115.10	−82.47	54	−65.85	43	−4.38	3
$(HCN)_2\cdots SnF_4$	−39.45	86.45	−73.19	58	−49.10	39	−3.61	3
$(HCN)_2\cdots PbF_4$	−31.06	58.31	−53.91	60	−32.26	36	−3.19	4

Table 8. AIM descriptors of the *cis* and *trans* complexes. Bond critical point (BCP) properties: electron density ρ, Laplacian of electron density $\nabla^2\rho$ and total electron energy (H) were obtained at the MP2/cc-pVTZ level. Data given in atomic units.

	interaction	ρ	$\nabla^2\rho$	H
	cis			
$(HCN)_2\cdots SiF_4$	F···N[a]	0.007	0.026	0.001
$(HCN)_2\cdots GeF_4$	Ge···N	0.012	0.042	0.001
$(HCN)_2\cdots SnF_4$	Sn···N	0.047	0.171	−0.005
$(HCN)_2\cdots PbF_4$	Sn···N	0.044	0.149	−0.004
	trans			
$(HCN)_2\cdots SiF_4$	Si···N	0.057	0.269	−0.013
$(HCN)_2\cdots GeF_4$	Ge···N	0.068	0.221	−0.020
$(HCN)_2\cdots SnF_4$	Sn···N	0.058	0.219	−0.010
$(HCN)_2\cdots PbF_4$	Sn···N	0.051	0.177	−0.006

[a] six equivalent interaction

their largest for the Ge···N bond. However, this point is clearly at odds with the interaction energies in Table 4 for which it is Sn and Pb which engage in the strongest bond with N, also true of the binding energies in Table 2. It might also be noted that AIM fails to identify a bond path between Si and N, observing only a very weak bond from N to each of the proximate F atoms of SiF_4.

The NBO scheme offers a useful means of analysing the charge transfers between orbitals and between subunits, along with their energetic implications. The sums of the second-order interaction energies E(2) between the lone electron pair of the nitrogen atoms LP(N) and the antibonding σ* (T–F) orbitals, as well as the total charge transfer (CT) from the two bases to the TF_4 subunit are collected in Table 9.

Table 9. NBO properties of *cis* and *trans* complexes obtained at the BLYP-D3/def2-TVZPP level.

	cis E(2)[a] [kcal/mol]	CT [me]	*trans* E(2)[a] [kcal/mol]	CT [me]
$(HCN)_2\cdots SiF_4$	1.2 (1.2)	0.2	35.2 (245.6)	306
$(HCN)_2\cdots GeF_4$	8.2 (8.6)	19	22.6 (149.9)	273
$(HCN)_2\cdots SnF_4$	46.8 (76.4)	163	28.1 (127.6)	244
$(HCN)_2\cdots PbF_4$	18.5 (58.2)	138	16.7 (84.0)	196

[a] Sum of E(2) between LP(N) and antibonding σ*(T–F); also including antibonding Rydberg (T) orbitals and "lone vacancy" LV(T) orbitals added in parentheses.

(Since there are also sizable charge transfers to Rydberg and lone pair vacancy orbitals within the NBO scheme, these transfers are also included in parentheses in Table 9.) One can observe parallels between the NBO quantities and the interaction energies in Table 4. First with regard to the *cis* complexes, the NBO parameters echo the Sn > Pb > Ge > Si ordering of E_{int}. The *trans* data are also parallel, with Pb engaged in the weakest trimer. NBO also agrees with the full energetics that the *trans* trimers are more strongly bound than their *cis* analogues. On the other hand, more detailed aspects are less than perfect. For example, CT for the *trans* structures would clearly suggest Si > Ge > Sn, whereas the energetics are less clear on this comparison. Since NBO does not simulate the total interaction energy but only its charge transfer aspects, one might choose to compare NBO quantities with the orbital interaction energies in Table 7. The correlations are stronger here. For example, the correlation coefficient for a linear fit of the charge transfers in Table 9 to E_{oi} in Table 7 is 0.96. An even better fit of 0.99 occurs when the (full) values of E(2) are correlated with E_{oi}.

3. Discussion

The majority of studies of tetrel bonding in the literature focus on the lighter C, Si, and Ge atoms. However, there are a few works dealing with tetravalent Sn and Pb, and the noncovalent bonds they form with various bases.[25,26,38,98,99] Previous studies have confirmed the trend that the tetrel bond grows stronger as T becomes larger,[30,32,33,47,100] but that the effect levels off between Sn and Pb.[45,101] An earlier work[45,102] supports the result noted here that the deformation energy induced within the Lewis acid molecule by formation of a tetrel bonded complex drops as the central tetrel atom grows in size. The ability of the heavier tetrel atoms to participate in two simultaneous noncovalent bonds is confirmed by earlier calculations[103] performed by Grabowski at the MP2 level, who also noted the possibility of both *trans* and *cis* structures, at least for Sn, for which the latter is more stable than the former by 3 kcal/mol, in nice agreement with our own findings. His data also support the larger interaction energies of Sn as

compared to Pb, as well as the higher deformation energies characteristic of the smaller Sn.

In order to accommodate and make room for a pair of bases, a normally tetrahedral TF_4 molecule must distort in one of two ways, but both based on the general octahedral skeleton. In the preferred structure, the two bases are situated *cis* to one another, leaving the original TF_4 segment in a sort of see-saw geometry. The energy required for this deformation of TF_4 is quite large for Si, nearly 100 kcal/mol, but drops quickly as T grows larger. On the positive side, the see-saw structure of TF_4 has a pair of intense σ-holes, each of which can form a strong tetrel bond with the base. The interaction energy of the two NCH molecules with the pre-distorted TF_4 is roughly 4 kcal/mol for Si, and rises to a maximum of 33 kcal/mol for Sn. When combined with the energy needed for this geometric deformation, the resulting binding energy is about 3–5 kcal/mol for Si and Ge, but 17 kcal/mol for the larger Sn and Pb which are not burdened with as large a distortion energy.

The other possible structure involves the placement of the two bases opposite one another in a *trans* arrangement. This sort of structure requires the deformation of the TF_4 into a D_{4h} planar structure which in turn involves a very sizable deformation energy. The latter is many times larger than that required to attain the pseudo see-saw geometry needed for the *cis* trimer. Also, the π-holes that lie above and below the T atom in the square geometry are somewhat less intense than the σ-holes of the *cis* structure. Nonetheless, the planar TF_4 structure allows a nearly unimpeded approach of the two bases toward the T atom, so the interaction energies are larger than in the *cis* arrangement, in the 36–46 kcal/mol range. But even these stronger intrinsic interactions are unable to overcome the very large deformation energy required to achieve a square planar structure. Consequently, the *trans* trimers are less tightly bound than their *cis* counterparts. This preference for the *cis* structure is quite sizable for the smaller T atoms, 22 kcal/mol for Si and 12 kcal/mol for Ge. However, the energy difference is reduced to only about 3 kcal/mol for the heavier Sn and Pb.

The shortness of some of the intermolecular T···N distances, barely more than 2.0 Å in some cases, leads to the question as to the most appropriate designation of these interactions. This distance is only about 10% larger than the sum of T and N covalent radii for the four *trans* geometries. Indeed, the same may be said of the *cis* trimers involving Sn and Pb. So in that sense, these complexes might be thought of as at least partially covalent. On the other hand, the various AIM parameters lie in the range of typical noncovalent bonds. And even the strongest of these interaction energies are less than 50 kcal/mol, arguing against a designation as a true covalent bond.

4. Conclusions

In conclusion, a tetrel atom in a tetravalent bonding situation is capable of engaging in a pair of noncovalent tetrel bonds simultaneously. The formation of these bonds leads the normally tetrahedral substituent arrangement to distort to an octahedral geometry. In the absence of external forces as might occur within a crystal environment or a macromolecule, the *cis* arrangement of the two bases is preferred to the *trans* configuration. This preference is most obvious for the smaller T atoms, but drops to only a small margin for the larger Sn and Pb atoms.

Acknowledgements

This work was financed in part by a statutory activity subsidy from the Polish Ministry of Science and Higher Education for the Faculty of Chemistry of Wroclaw University of Science and Technology. A generous computer time from the Wroclaw Supercomputer and Networking Center is acknowledged.

Conflict of Interest

The authors declare no conflict of interest.

Keywords: density functional calculations · donor–acceptor systems · σ-hole · π-hole, molecular modelling

[1] M. Iwaoka, S. Takemoto, S. Tomoda, *J. Am. Chem. Soc.* **2002**, *124*, 10613–10620.
[2] G. R. Desiraju, V. Nalini, *J. Mater. Chem.* **1991**, *1*, 201–203.
[3] P. Auffinger, F. A. Hays, E. Westhof, P. S. Ho, *Proc. Natl. Acad. Sci. USA* **2004**, *101*, 16789–16794.
[4] P. Politzer, J. S. Murray, P. Lane, *Int. J. Quantum Chem.* **2007**, *107*, 3046–3052.
[5] J. E. Del Bene, I. Alkorta, J. Elguero, In *Noncovalent Forces*, Scheiner, S., Ed. Springer: Dordrecht, Netherlands, **2015**, Vol. *19*, pp 191–263.
[6] P. Politzer, J. S. Murray, In *Noncovalent Forces*, S. Scheiner, Ed. Springer: Dordrecht, Netherlands, **2015**, Vol. *19*, pp 357–389.
[7] S. Scheiner, *Acc. Chem. Res.* **2013**, *46*, 280–288.
[8] S. Benz, A. I. Poblador-Bahamonde, N. Low-Ders, S. Matile, *Angew. Chem. Int. Ed.* **2018**, *57*, 5408–5412; *Angew. Chem.* **2018**, *130*, 5506–5510.
[9] S. J. Grabowski, *Phys. Chem. Chem. Phys.* **2017**, *19*, 29742–29759.
[10] A. Karim, N. Schulz, H. Andersson, B. Nekoueishahraki, A.-C. C. Carlsson, D. Sarabi, A. Valkonen, K. Rissanen, J. Gräfenstein, S. Keller, M. Erdélyi, *J. Am. Chem. Soc.* **2018**, *140*, 17571–17579.
[11] V. R. Mundlapati, D. K. Sahoo, S. Bhaumik, S. Jena, A. Chandrakar, H. S. Biswal, *Angew. Chem. Int. Ed.* **2018**, *57*, 16496–16500.
[12] R. C. Trievel, S. Scheiner, *Molecules* **2018**, *23*, 2965–2981.
[13] X. García-Llinás, A. Bauzá, S. K. Seth, A. Frontera, *J. Phys. Chem. A* **2017**, *121*, 5371–5376.
[14] A. Bauzá, A. Frontera, *Cryst.* **2016**, *6*, 26.
[15] S. P. Thomas, M. S. Pavan, T. N. Guru Row, *Chem. Commun.* **2014**, *50*, 49–51.
[16] A. Frontera, A. Bauzá, *Chem. Eur. J.* **2018**, *24*, 16582–16587.
[17] C. Packianathan, P. Kandavelu, B. P. Rosen, *Biochem.* **2018**, *57*, 4083–4092.
[18] M. B. Poulin, J. L. Schneck, R. E. Matico, P. J. McDevitt, M. J. Huddleston, W. Hou, N. W. Johnson, S. H. Thrall, T. D. Meek, V. L. Schramm, *Proc. Natl. Acad. Sci. USA* **2016**, *113*, 1197–1201.
[19] R. J. Fick, M. C. Clay, L. Vander Lee, S. Scheiner, H. Al-Hashimi, R. C. Trievel, *Biochem.* **2018**, *57*, 3733–3740.
[20] J. Zhang, J. P. Klinman, *J. Am. Chem. Soc.* **2016**, *138*, 9158–9165.
[21] I. Ali, H. Ramage, D. Boehm, L. M. A. Dirk, N. Sakane, K. Hanada, S. Pagans, K. Kaehlcke, K. Aull, L. Weinberger, R. Trievel, M. Schnoelzer, M. Kamada, R. Houtz, M. Ott, *J. Biol. Chem.* **2016**, *291*, 16240–16248.
[22] I. Alkorta, A. Legon, *Molecules* **2018**, *23*, 2250.
[23] I. Alkorta, J. Elguero, J. E. Del Bene, *ChemPhysChem.* **2018**, *19*, 1886–1894.
[24] A. C. Legon, *Phys. Chem. Chem. Phys.* **2017**, *19*, 14884–14896.

[25] A. Bauzá, T. J. Mooibroek, A. Frontera, *Chem. Rec.* **2016**, *16*, 473–487.
[26] P. Matczak, *Struct. Chem.* **2015**, *26*, 301–318.
[27] D. Mani, E. Arunan, *J. Phys. Chem. A* **2014**, *118*, 10081–10089.
[28] M. Marín-Luna, I. Alkorta, J. Elguero, *Theor. Chem. Acc.* **2017**, *136*, 41–48.
[29] M. D. Esrafili, H. Kiani, F. Mohammadian-Sabet, *Mol. Phys.* **2016**, *114*, 3658–3668.
[30] S. Scheiner, *J. Phys. Chem. A* **2017**, *121*, 5561–5568.
[31] D. Sethio, V. Oliveira, E. Kraka, *Molecules* **2018**, *23*, 2763.
[32] Y. Wei, Q. Li, *Mol. Phys.* **2018**, *116*, 222–230.
[33] Y.-X. Wei, H.-B. Li, J.-B. Cheng, W.-Z. Li, Q.-Z. Li, *Int. J. Quantum Chem.* **2017**, *117*, e25448.
[34] S. J. Grabowski, *Phys. Chem. Chem. Phys.* **2014**, *16*, 1824–1834.
[35] M. Esrafili, P. Mousavian, *Molecules* **2018**, *23*, 2642.
[36] M. D. Esrafili, S. Asadollahi, P. Mousavian, *Chem. Phys. Lett.* **2018**, *691*, 394–400.
[37] M. Ghara, S. Pan, A. Kumar, G. Merino, P. K. Chattaraj, *J. Comput. Chem.* **2016**, *37*, 2202–2211.
[38] M. Liu, Q. Li, J. Cheng, W. Li, H.-B. Li, *J. Chem. Phys.* **2016**, *145*, 224310.
[39] J. E. Del Bene, I. Alkorta, J. Elguero, *Chem. Phys. Lett.* **2016**, *655–656*, 115–119.
[40] M. Liu, Q. Li, S. Scheiner, *Phys. Chem. Chem. Phys.* **2017**, *19*, 5550–5559.
[41] A. Bauza, T. J. Mooibroek, A. Frontera, *Chem. Commun.* **2014**, *50*, 12626–12629.
[42] S. Scheiner, *J. Phys. Chem. A* **2015**, *119*, 9189–9199.
[43] E. Solel, S. Kozuch, *Molecules* **2018**, *23*, 2742.
[44] W. Zierkiewicz, M. Michalczyk, S. Scheiner, *Phys. Chem. Chem. Phys.* **2018**, *20*, 8832–8841.
[45] S. Scheiner, *J. Phys. Chem. A* **2018**, *122*, 2550–2562.
[46] S. J. Grabowski, W. A. Sokalski, *ChemPhysChem.* **2017**, *18*, 1569–1577.
[47] M. Liu, Q. Li, W. Li, J. Cheng, *Struct. Chem.* **2017**, *28*, 823–831.
[48] J. E. Del Bene, I. Alkorta, J. Elguero, *J. Phys. Chem. A* **2017**, *121*, 8136–8146.
[49] S. Scheiner, *Chem. Phys. Lett.* **2019**, *714*, 61–64.
[50] S. Scheiner, *J. Phys. Chem. A* **2018**, *122*, 7852–7862.
[51] A. C. Tagne Kuate, M. M. Naseer, M. Lutter, K. Jurkschat, *Chem. Commun.* **2018**, *54*, 739–742.
[52] G. Mahmoudi, A. Bauza, M. Amini, E. Molins, J. T. Mague, A. Frontera, *Dalton Trans.* **2016**, *45*, 10708–10716.
[53] G. Mahmoudi, A. Bauza, A. Frontera, *Dalton Trans.* **2016**, *45*, 4965–4969.
[54] S. Roy, M. G. B. Drew, A. Bauza, A. Frontera, S. Chattopadhyay, *New J. Chem.* **2018**, *42*, 6062–6076.
[55] A. Bauzá, T. J. Mooibroek, A. Frontera, *Angew. Chem. Int. Ed.* **2013**, *52*, 12317–12321; *Angew. Chem.* **2013**, *125*, 12543–12547.
[56] S. Scheiner, *Chem. Eur. J.* **2016**, *22*, 18850–18858.
[57] S. Scheiner, *J. Phys. Chem. A* **2017**, *121*, 3606–3615.
[58] S. Scheiner, *Faraday Discuss.* **2017**, *203*, 213–226.
[59] S. Scheiner, *Molecules* **2018**, *23*, 1147–1155.
[60] S. Scheiner, *Molecules* **2019**, *24*, 227.
[61] S. J. Grabowski, *Chem. Phys. Lett.* **2014**, *605–606*, 131–136.
[62] G. J. Buralli, D. J. R. Duarte, G. L. Sosa, N. M. Peruchena, *Struct. Chem.* **2017**, *28*, 1823–1830.
[63] W. Wang, *J. Phys. Chem. A* **2011**, *115*, 9294–9299.
[64] O. Kirshenboim, S. Kozuch, *J. Phys. Chem. A* **2016**, *120*, 9431–9445.
[65] V. d. P. N. Nziko, S. Scheiner, *J. Phys. Chem. A* **2014**, *118*, 10849–10856.
[66] M. D. Esrafili, F. Mohammadian-Sabet, *Struct. Chem.* **2016**, *27*, 617–625.
[67] M. D. Esrafili, R. Nurazar, *Mol. Phys.* **2016**, *114*, 276–282.
[68] M. D. Esrafili, N. Mohammadirad, *Struct. Chem.* **2016**, *27*, 939–946.
[69] B. Khalili, M. Rimaz, *Struct. Chem.* **2017**, *28*, 1065–1079.
[70] M. D. Esrafili, E. Vessally, *Chem. Phys. Lett.* **2016**, *662*, 80–85.
[71] M. Gawrilow, H. Beckers, S. Riedel, L. Cheng, *J. Phys. Chem. A* **2018**, *122*, 119–129.
[72] A. Bauza, A. Frontera, *Phys. Chem. Chem. Phys.* **2015**, *17*, 24748–24753.
[73] A. Bauzá, A. Frontera, *ChemPhysChem.* **2015**, *16*, 3625–3630.
[74] S. Scheiner, J. Lu, *Chem. Eur. J.* **2018**, *24*, 8167–8177.
[75] The Cambridge Structural Database: C. R. Groom, I. J. Bruno, M. P. Lightfoot, S. C. Ward, *Acta Crystallogr.* **2016**, *B72*, 171.
[76] A. W. Waller, N. M. Weiss, D. A. Decato, J. A. Phillips, *J. Mol. Struct.*, **2017**, *1130*, 984–993.
[77] D. T. Tran, P. Y. Zavalij, S. R. J. Oliver, *Acta Crystallogr. Sect. E: Structure Reports Online* **2002**, *58*, m742.
[78] C. Møller, M. S. Plesset, *Phys. Rev.* **1934**, *46*, 618.
[79] T. H. Dunning Jr., *J. Chem. Phys.* **1989**, *90*, 1007.
[80] A. D. Becke, *J. Chem. Phys.* **1993**, *98*, 5648–5652.
[81] K. Raghavachari, G. W. Trucks, J. A. Pople, M. Head-Gordon, *Chem. Phys. Lett.* **1989**, *157*, 479.
[82] C. Lee, W. Yang, R. G. Parr, *Phys. Rev. B* **1988**, *37*, 785–789.
[83] F. Weigend and R. Ahlrichs, *Phys. Chem. Chem. Phys.* **2005**, *7*, 3297–305.
[84] F. Weigend, *Phys. Chem. Chem. Phys.* **2006**, *8*, 1057–65.
[85] D. Feller, *J. Comb. Chem.* **1996**, *17*, 1571.
[86] K. A. Peterson, *J. Chem. Phys.* **2003**, *119*, 11099.
[87] S. F. Boys and F. Bernardi, *Mol. Phys.* **1970**, *19*, 553.
[88] M. J. Frisch, G. W. Trucks, H. B. Schlegel, G. E. Scuseria, M. A. Robb, J. R. Cheeseman, G. Scalmani, V. Barone, B. Mennucci, G. A. Petersson, H. Nakatsuji, M. Caricato, X. Li, H. P. Hratchian, A. F. Izmaylov, J. Bloino, G. Zheng, J. L. Sonnenberg, M. Hada, M. Ehara, K. Toyota, R. Fukuda, J. Hasegawa, M. Ishida, T. Nakajima, Y. Honda, O. Kitao, H. Nakai, T. Vreven, J. A. Montgomery Jr., J. E. Peralta, F. Ogliaro, M. Bearpark, J. J. Heyd, E. Brothers, K. N. Kudin, V. N. Staroverov, R. Kobayashi, J. Normand, K. Raghavachari, A. Rendell, J. C. Burant, S. S. Iyengar, J. Tomasi, M. Cossi, N. Rega, J. M. Millam, M. Klene, J. E. Knox, J. B. Cross, V. Bakken, C. Adamo, J. Jaramillo, R. Gomperts, R. E. Stratmann, O. Yazyev, A. J. Austin, R. Cammi, C. Pomelli, J. W. Ochterski, R. L. Martin, K. Morokuma, V. G. Zakrzewski, G. A. Voth, P. Salvador, J. J. Dannenberg, S. Dapprich, A. D. Daniels, O. Farkas, J. B. Foresman, J. V. Ortiz, J. Cioslowski and D. J. Fox, Gaussian 09, Gaussian, Inc., Wallingford CT, **2009**.
[89] G. te Velde, F. M. Bickelhaupt, E. J. Baerends, C. Fonseca Guerra, S. J. A. van Gisbergen, J. G. Snijders, T. Ziegler, *J. Comput. Chem.* **2001**, *22*, 931.
[90] C. Fonseca Guerra, J. G. Snijders, G. te Velde, E. J. Baerends, *Theor. Chem. Acc.* **1998**, *99*, 391.
[91] ADF2014, SCM, Theoretical Chemistry, Vrije Universiteit, Amsterdam, The Netherlands, http://www.scm.com.
[92] F. Bulat, A. Toro-Labbe, T. Brinck, J. S. Murray and P. Politzer, *J. Mol. Model.* **2010**, *16* 1679.
[93] T. Lu, F. Chen, *J. Comput. Chem.* **2012**, *33*, 580.
[94] T. Lu, F. Chen, *J. Mol. Graphics Modell.* **2012**, *38*, 314–323.
[95] AIMAll (Version 14.11.23), Todd A. Keith, TK Gristmill Software, Overland Park KS, USA, 2014 (aim.tkgristmill.com)
[96] E. D. Glendening, C. R. Landis, F. Weinhold, *J. Comput. Chem.* **2013**, *34*, 1429–1437.
[97] S. Alvarez, *Dalton Trans.* **2013**, *42*, 8617.
[98] P. Matczak, *Comput. Theor. Chem.* **2015**, *1051*, 110–122.
[99] G. Mahmoudi, A. Bauza, A. Frontera, P. Garczarek, V. Stilinovic, A. M. Kirillov, A. Kennedy, C. Ruiz-Perez, *CrystEngComm* **2016**, *18*, 5375–5385.
[100] W. Zierkiewicz, M. Michalczyk, S. Scheiner, *Molecules* **2018**, *23*, 1416.
[101] K. J. Donald, M. Tawfik, *J. Phys. Chem. A* **2013**, *117*, 14176–14183.
[102] S. J. Grabowski, *Crystals* **2017**, *7*, 43.
[103] S. J. Grabowski, *Appl. Organomet. Chem.* **2017**, e3727.
[104] G. A. Koutsantonis, T. S. Morien, B. W. Skelton, A. H. White, *Acta Crystallogr. Sect. C: Cryst.Struct.Commun.* **2003**, *59*, m361.
[105] F. R. Fronczek, CSD Communication (Private Communication), **2015**.
[106] M. F. Davis, M. Clarke, W. Levason, G. Reid, M. Webster, *Eur. J. Inorg. Chem.* **2006**, 2773.
[107] F. Cheng, M. F. Davis, A. L. Hector, W. Levason, G. Reid, M. Webster, Wenjian Zhang, *Eur. J. Inorg. Chem.* **2007**, 4897.
[108] L. M. Engelhardt, J. M. Patrick, C. R. Whitaker, A. H. White, *Aust. J. Chem.* **1987**, *40*, 2107.
[109] V. A. Bain, R. C. G. Killean, M. Webster, *Acta Crystallogr. Sect. B: Struct. Crystallogr. Cryst. Chem.* **1969**, *25*, 156.
[110] N. W. Mitzel, K. Vojinovic, T. Foerster, H. E. Robertson, K. B. Borisenko, D. W. H. Rankin, *Chem. Eur. J.* **2005**, *11*, 5114.
[111] O. J. Rutt, A. R. Cowley, S. J. Clarke, *Acta Crystallogr. Sect. E: Struct. Rep. Online* **2007**, *63*, o3406.

Manuscript received: February 26, 2019
Revised manuscript received: February 15, 2019
Accepted manuscript online: February 15, 2019
Version of record online: March 7, 2019